Published in final edited form as:
Neuron. 2011 September 8; 71(5): 858–868. doi:10.1016/j.neuron.2011.06.035.

Rapid target-specific remodeling of fast-spiking inhibitory circuits after loss of dopamine

Aryn H. Gittis[1], **Giao B. Hang**[1], **Eva S. LaDow**[1,2], **Liza R. Shoenfeld**[1], **Bassam V. Atallah**[3], **Steven Finkbeiner**[1,4], and **Anatol C. Kreitzer**[1,4,*]

[1]Gladstone Institute of Neurological Disease

[2]Pharmacogenomics and Pharmaceutical Sciences Program

[3]Neuroscience Graduate Program and Neurobiology Section, Division of Biology, University of California, San Diego

[4]Departments of Physiology and Neurology, University of California, San Francisco

Summary

In Parkinson disease (PD), dopamine depletion alters neuronal activity in the direct and indirect pathways and leads to increased synchrony in the basal ganglia network. However, the origins of these changes remain elusive. Because GABAergic interneurons regulate activity of projection neurons and promote neuronal synchrony, we recorded from pairs of striatal fast-spiking (FS) interneurons and direct- or indirect-pathway MSNs after dopamine depletion with 6-OHDA. Synaptic properties of FS-MSN connections remained similar, yet within 3 days of dopamine depletion, individual FS cells doubled their connectivity to indirect-pathway MSNs, whereas connections to direct-pathway MSNs remained unchanged. A model of the striatal microcircuit revealed that such increases in FS innervation were effective at enhancing synchrony within targeted cell populations. These data suggest that after dopamine depletion, rapid target-specific microcircuit organization in the striatum may lead to increased synchrony of indirect-pathway MSNs that contributes to pathological network oscillations and motor symptoms of PD.

Introduction

The input nucleus of the basal ganglia, the striatum, contains two major populations of projection neurons, known as medium spiny neurons (MSNs), which differ in their gene expression and axonal projection targets (Bolam et al., 2000; Smith et al., 1998). MSNs that express dopamine D1 receptors (D1 MSNs) form the direct pathway, which promotes movement. MSNs that express dopamine D2 receptors (D2 MSNs) form the origin of the indirect pathway, which suppresses movement (Bolam et al., 2000; Kravitz et al., 2010; Kreitzer, 2009; Smith et al., 1998). Changes in direct and indirect pathway basal ganglia circuits have been proposed to underlie motor deficits in Parkinson's disease (PD) (Albin et al., 1989; DeLong, 1990; Galvan and Wichmann, 2007; Graybiel et al., 1994). However, the

*To whom correspondence should be addressed: Gladstone Institute of Neurological Disease, 1650 Owens St., San Francisco, CA 94158, Tel: 415-734-2507, Fax: 415-355-0824, akreitzer@gladstone.ucsf.edu.

pathophysiological mechanisms that alter basal ganglia output after loss of dopamine are not well understood.

One proposed mechanism for altered activity in the direct and indirect pathways after loss of dopamine is the dysregulation of long-term potentiation (LTP) and long-term depression (LTD) at excitatory afferents to D1 and D2 MSNs (Calabresi et al., 2007; Kreitzer and Malenka, 2008; Lovinger, 2010; Shen et al., 2008). Dysregulation of plasticity could contribute to enhanced excitatory drive onto D2 MSNs, leading to a net suppression of movement that may contribute to hypokinetic features of PD. Although firing rate changes in the direct and indirect pathways can regulate parkinsonian motor behaviors (Kravitz et al., 2010), mechanisms other than firing rate could alter basal ganglia output. For example, even without a net increase in firing rate, enhanced synchrony in an afferent population can lead to increased excitation (or inhibition) of target neurons by temporal coordination of inputs (Burkhardt et al., 2007; Mallet et al., 2008a). Indeed, changes in synchrony among MSNs have been observed in the striatum after loss of dopamine (Burkhardt et al., 2007; Costa et al., 2006; Jaidar et al., 2010), and altered neuronal synchrony is observed in other indirect-pathway nuclei (globus pallidus and subthalamic nucleus) in PD models (Bevan et al., 2002; Brown, 2003; Hammond et al., 2007; Hutchison et al., 2004; Terman et al., 2002). Aberrant synchrony would therefore enhance the influence of the indirect pathway on basal ganglia output nuclei and exacerbate parkinsonian motor deficits.

Fast-spiking (FS) interneurons play an important role in coordinating neuronal synchrony in numerous brain regions (Bartos et al., 2007; Cobb et al., 1995; Fuchs et al., 2007; Sohal et al., 2009; Tamas et al., 2000), including the striatum (Berke et al., 2004). In the striatum, FS interneurons represent the main source of feedforward inhibition on MSNs (Gittis et al., 2010; Koos et al., 2004; Planert et al., 2010) and are therefore well-positioned to control neuronal synchrony. Single FS interneurons inhibit both direct-and indirect-pathway MSNs, but under normal conditions are more likely to synapse onto direct-pathway MSNs (Gittis et al., 2010). The recent finding that GABAergic interneurons in the hippocampus also display target-specificity (Varga et al., 2010) suggests that this may be an important feature of GABAergic networks that helps to establish pathway-specific processing. Acute increases in dopamine affect excitability and synaptic properties of FS interneurons (Bracci et al., 2002; Centonze et al., 2003) but little is known about how chronic decreases in dopamine signaling, as experienced during PD, affect FS microcircuits.

To test the hypothesis that changes in striatal FS microcircuits contribute to basal ganglia dysfunction induced by dopamine depletion, we examined the synaptic properties and connectivity of FS interneurons in the striatum of control and dopamine-depleted mice. Although no changes were observed in synaptic properties at FS-MSN unitary synapses, a significant shift in microcircuit organization occurred, with FS cells nearly doubling their rate of connectivity onto indirect-pathway D2 MSNs. Using a simple model of the striatal feedforward microcircuit, we show that the selective enhancement of FS innervation of D2 MSNs produced by dopamine depletion is sufficient to increase synchrony in these indirect pathway projection neurons. These data demonstrate that the target-specificity of FS GABAergic interneurons is under dynamic control, which may have important implications for microcircuit function and behavior in disease states.

Results

FS interneurons increase connectivity selectively onto D2 MSNs after dopamine depletion

To deplete dopamine in the striatum, 6-hydroxydopamine (6-OHDA) was injected unilaterally into the medial forebrain bundle (MFB) of 3–4-week-old mice. By performing unilateral depletions, dopamine could be selectively reduced by > 95% in one hemisphere,

allowing mice to remain relatively healthy with low mortality rates (Supplemental Fig. 1 and see methods). To identify GABAergic interneurons, D1 and D2 MSNs in a single slice, we used mice that were the offspring of a cross between the Lhx6-EGFP BAC line (labels GABAergic interneurons with GFP) and the Drd1a-tdTomato BAC line (labels D1 MSNs with RFP; (Shuen et al., 2008). As previously established, this cross enables the accurate identification of GABAergic interneurons, D1 and D2 MSNs in a single slice (see methods and (Gertler et al., 2008; Gittis et al., 2010; Matamales et al., 2009). FS interneurons were targeted using GFP fluorescence and their identity was confirmed in the whole-cell recording configuration based on their firing properties (Gittis et al., 2010). The excitability of FS interneurons was not changed by dopamine depletion (Supplementary Fig. 2).

To determine whether dopamine depletion changes connectivity of FS interneurons onto D1 and D2 MSNs, paired recordings were performed in slices from saline- and 6-OHDA-injected mice. Experiments were initiated by establishing a whole-cell recording from an FS interneuron, then testing its connectivity with as many neighboring MSNs as possible until the presynaptic interneuron was lost. Typically 1–6 (average 2.4) MSNs were sampled per interneuron.

The probability of finding a synaptic connection between FS-D1 MSN pairs was not changed by dopamine depletion. Connection probability was 0.60 in saline-injected mice (average distance between pairs = 113 ± 49 μm) and 0.53 in 6-OHDA-injected mice (average distance between pairs = 105 ± 50.1 μm) ($p = 0.60$) (Fig. 1A). In contrast, dopamine depletion significantly increased the probability of finding a synaptic connection between FS-D2 MSN pairs. In saline-injected mice, connection probability was 0.39 (average distance between pairs = 116 ± 46 μm) but was nearly 2-fold higher, 0.77, in 6-OHDA-injected mice (average distance between pairs = 101 ± 48 μm) ($p = 0.0004$). Changes in FS connectivity occurred rapidly after dopamine depletion, with increased connectivity onto D2 MSNs already present at 3 days after dopamine depletion (Fig. 1B – C). Importantly, the observed change in connection probability was not due to a difference in the number of healthy ‘patchable’ D1 versus D2 MSNs in the slice after dopamine depletion. In six slices from a total of two 6-OHDA-injected mice, we counted 43 ± 7 patchable D1 MSNs and 40 ± 8 patchable D2 MSNs surrounding FS interneurons. In six slices from two saline-injected mice, we counted 43 ± 10 patchable D1 MSNs and 42 ± 6 D2 patchable MSNs surrounding FS interneurons.

As shown in Fig. 1D–G, dopamine depletion did not change the properties of unitary inhibitory postsynaptic currents (uIPSCs) recorded in MSNs. Action potentials evoked in presynaptic FS interneurons with brief somatic current injections (5 ms, typically ~1 nA) reliably elicited uIPSCs in postsynaptic MSNs (Fig. 2D). Amplitudes of uIPSCs were similar from trial-to-trial for a given pair but varied widely across the population (Fig. 2E). The amplitudes of uIPSCs were not significantly different across conditions ($p_{D1} = 0.94$; $p_{D2} = 0.20$, Wilcoxon) (Fig. 2E). These data demonstrate that postsynaptic GABA receptors at FS-MSN synapses are not altered after dopamine depletion.

To determine whether aspects of presynaptic function were affected by dopamine depletion, action potentials were elicited in presynaptic FS interneurons at frequencies of 10, 20, 50, or 100 Hz (Fig. 2F–G). Short-term dynamics were measured as the change in amplitude of uIPSCs that accumulated during trains of 10 action potentials at each frequency. Synapses exhibited frequency-independent depression, to 20–40% their initial amplitudes, across all frequencies tested. The extent of this depression was similar in D1 and D2 MSNs and did not differ significantly between saline- and 6-OHDA-injected mice ($p > 0.05$ at all frequencies) (Fig. 2G). This demonstrates that dopamine depletion does not significantly change the presynaptic dynamics of FS synapses onto MSNs.

FS connectivity is not changed by acute blockade of dopamine receptors

At least two mechanisms could account for the increased synaptic connectivity observed from FS interneurons onto D2 MSNs in 6-OHDA-injected mice: (1) unsilencing of preexisting synapses (Foldy et al., 2007), for example if tonic dopamine levels under control conditions reduced release probability or (2) formation of new synapses.

To determine whether tonic levels of dopamine in the slice exert a silencing effect at FS-MSN synapses, dopamine signaling was acutely blocked by bath perfusion of D1 and D2 antagonists (5 μM SCH23390 and 10 μM sulpiride, respectively). Acute blockade of dopamine signaling did not significantly alter FS-MSN connection probabilities relative to vehicle control (1:10,000 DMSO in ACSF) (Fig. 1A). Connection probabilities onto D1 MSNs were 0.59 (distance = 119 ± 50 μm) compared to 0.55 in control (distance = 111 ± 45 μm) ($p = 0.77$) and connection probabilities onto D2 MSNs were 0.42 (distance = 108 ± 51 μm) compared to 0.38 in control (distance = 106 ± 48 μm) ($p = 0.81$) (Fig. 2A).

Similarly, dopamine antagonists did not significantly change the amplitudes or short-term dynamics of uIPSCs onto MSNs. In the presence of dopamine antagonists, average uIPSC amplitudes in D1 MSNs were 400 ± 514 pA, n = 12, compared to 486 ± 442 pA, n = 15 in control ($p = 0.20$, Wilcoxon) and in D2 MSNs were 442 ± 527 pA, n = 10 compared to 425 ± 391 pA, n = 8 in control, $p = 0.96$, Wilcoxon) (Fig. 2B). Shortterm plasticity, measured as synaptic depression during trains of 10 action potentials at 10, 20, 50, and 100 Hz was also not changed by dopamine antagonists ($p > 0.05$ at all frequencies) (Fig. 3C – D). From these data, we conclude that tonic dopamine levels in the slice do not reduce connection probability or synaptic properties of FS-MSN synapses and therefore do not exert a silencing effect at FS-MSN synapses.

FS axons sprout after dopamine depletion

To test whether increased FS- D2 MSN connectivity observed in 6-OHDA-injected mice results from sprouting of FS axons, we examined FS interneuron morphology within one week after injections with saline or 6-OHDA. Slices from 5 mice injected with 6-OHDA and 4 mice injected with saline were used for this analysis. Figure 3A – E shows examples of FS interneurons filled with biocytin and reconstructed with Neurolucida software. Axons were distinguished from dendrites by their thinner diameter and beaded appearance (Suzuki and Bekkers, 2010). Neurons in both saline- and 6-OHDA-injected mice had dense axonal arborizations and aspiny dendrites concentrated within a 200 – 400 μm radius, characteristic of FS interneurons (Kawaguchi, 1993).

Quantification of axonal and dendritic lengths revealed that the total length of FS axons was significantly greater in 6-OHDA-injected mice (14.53 ± 4.46 mm, n = 9), relative to saline-injected mice (8.98 ± 5.88 mm, n = 11, $p = 0.04$, Wilcoxon) (Fig. 3F). However, there was no significant change in dendritic length (1.62 ± 0.78 mm, n = 9 in 6-OHDA-injected mice vs. 2.06 ± 0.90 mm, n = 11 in saline-injected mice, $p = 0.11$) (Fig. 3G).

Differences in axonal morphology of FS interneurons between saline- and 6-OHDA-injected mice were further characterized using a Sholl analysis (Fig. 3E). Dopamine depletion did not change the average distance over which FS axons extended, measured by the maximum radius at which crossings were detected. On average, crossings of FS axons were detected up to 320 ± 103 μm away from the soma in saline-injected mice (n = 11) and up to 320 ± 81 μm away from the soma in 6-OHDA-injected mice (n = 9) (Fig. 3H).

In contrast, there was a significant increase in the number of grid crossings by FS axons in dopamine-depleted striatum relative to control. The number of crossings was higher in 6-OHDA-injected mice (535 ± 143, n = 9) compared to saline-injected mice (364 ± 234, n =

11, p = 0.04, 1-tailed Wilcoxon) (Fig. 3I). In summary, morphological analyses revealed that the axonal arbors of FS interneurons are denser and more complex after dopamine depletion, supporting the hypothesis that FS axons form new synapses onto D2 MSNs after dopamine depletion.

FS synapses onto D2 MSNs increase after dopamine depletion

To confirm that increases in FS axons correspond to increases in FS presynaptic terminals, we performed immunostains against the vesicular GABA transporter (vGAT) to label inhibitory presynaptic terminals, and against parvalbumin (PV) to label processes from FS interneurons. In 6-OHDA injected mice, colocalization between vGAT and PV was increased relative to saline-injected mice (Fig. 4A–C). In saline-injected mice, 12.3 ± 3.0% of vGAT pixels colocalized with PV, but in 6-OHDA-injected mice, 20.1 ± 3.6% of vGAT pixels colocalized with PV ($p < 0.0001$). These data demonstrate that there are significantly more inhibitory terminals from FS interneurons in 6-OHDA-injected mice compared to saline-injected mice.

To determine whether increases in FS terminals were pathway-specific, we performed a second analysis, taking advantage of the basket-like synapses formed by FS interneurons around the soma of MSNs (Bolam et al., 2000; Kawaguchi et al., 1995). Experiments were performed in D2-GFP BAC transgenic mice to differentiate somata of D1 and D2 MSNs. As shown in Fig. 4D–F, the number of PV/vGAT puncta around the somata of D2 MSNs was significantly increased in 6-OHDA-injected mice relative to saline-injected mice (9.5 ± 3.3, n = 15 vs. 6.3 ± 1.9, n = 15, p = 0.003). In contrast, there was no significant difference in the number of PV/vGAT puncta around the somata of D1 MSNs (9.8 ± 2.6, n = 15 in 6-OHDA-injected mice vs. 9.9 ± 2.2, n = 15 in saline-injected mice, p = 0.81) (Fig. 4G – I). Combined with morphological data from Fig. 3, these results suggest that pathway-specific increases in FS connectivity onto D2 MSNs after dopamine depletion are mediated by sprouting of FS axons and formation of new FS synapses onto D2 MSNs.

mIPSC frequency reveals increased inhibition onto D2 MSNs after dopamine depletion

To functionally test whether individual D2 MSNs receive more convergent inhibition after dopamine depletion, miniature IPSCs (mIPSCs) were recorded in D1 and D2 MSNs within one week after surgery. During slice experiments, mIPSCs were recorded in the presence of 5 μM NBQX and 1 μM TTX to block glutamatergic transmission and spontaneous activity, respectively. At a holding potential of −80 mV, mIPSCs were easily visible in MSNs (Fig. 5A&D). The majority of these events likely arise from FS interneurons, which have high rates of spontaneous release (Bacci et al., 2003; Xiang et al., 2002) and form more numerous connections onto MSNs then other cell types (Gittis et al., 2010; Taverna et al., 2008).

In saline-injected mice, the frequency of mIPSCs was significantly higher onto D1 MSNs than D2 MSNs ($p = 0.02$, Fig. 5H) mirroring the higher connection probability normally observed between FS interneurons and D1 MSNs (Fig. 1A). Mice injected with 6-OHDA showed no significant difference in mIPSC amplitudes (Fig. 5B, E, G) but showed a nearly two-fold increase in mIPSC frequencies selectively onto D2 MSNs ($p = 0.0007$) (Fig. 5F&H). The lack of change in mIPSC amplitude distribution after dopamine depletion (and enhanced FS innervation) indicates that mIPSCs recorded from MSNs arise predominantly from FS inputs, both before and after dopamine depletion. The increase in mIPSC frequency selectively onto D2 MSNs is consistent with increased innervation from FS interneurons. However, given the lack of increase in uIPSC amplitude (Fig. 1E), these data suggest that for any given FS-MSN pair, the number of synapses formed is stereotyped. Thus, pre-existing FS-MSN pairs were not significantly strengthened, whereas new FS-MSN pairs were connected, on average, by similar numbers of synapses as pre-existing pairs.

To determine whether changes in inhibitory innervation persist beyond 1 week, we measured mIPSCs in mice 2 weeks and 1 month after injections. Similar to data at 1 week, we observed changes in mIPSC frequency (but not amplitude) selectively onto D2 MSNs (Supplemental Fig. 3). In saline-injected mice, mIPSC frequency was higher onto D1 MSNs than D2 MSNs. In 6-OHDA-injected mice, mIPSC frequency onto D2 MSNs was significantly increased at 2 weeks ($p < 0.0001$) and 1 month ($p = 0.003$). These data suggest that increased innervation of D2 MSNs by FS interneurons persists for at least 1 month.

Selective increase in feedforward inhibition may enhance synchrony of D2 MSNs

To probe how increased connections from FS interneurons onto D2 MSNs can affect striatal function, we utilized a simple model of the striatal microcircuit (Fig. 6A). MSNs and FS interneurons were modeled as single-compartment neurons with intrinsic properties that matched experimental data (see methods). Individual FS interneurons connected to D1 and D2 MSNs with connection probabilities based on data from Fig. 1 (connection probabilities in the control model network were 0.5 for FS-D1 MSNs and 0.39 for FS-D2 MSNs; connection probabilities in the dopamine-depleted model network were 0.5 for FS-D1 MSNs and 0.77 for FS-D2 MSNs), and D1 and D2 MSNs were interconnected with connection probabilities based on Taverna et al., 2008. GABAergic FS innervations of MSNs was considered to inhibit MSN spiking both before and after dopamine depletion, as observed experimentally (Mallet et al., 2006).

In the control network, there was little synchrony in either MSN population (Fig. 6B–C). At time 0, the average z-score for D1-D1 pairs was 0.28 ± 0.03 and that of D2-D2 pairs was 0.18 ± 0.03. When FS connectivity onto D2 MSNs was increased in the dopamine-depleted network, marked synchrony emerged between D2 MSNs. Aberrant synchrony in the D2 MSN population—but not the D1 MSN population—can be seen in figure 6D. This aberrant synchrony among D2 MSNs was apparent in the population cross-correlogram (Fig. 6E). At time 0, the z-score of the D2 MSN population was 1.0 ± 0.04, significantly greater than in the control network ($p < 0.0001$). In contrast, synchrony among D1 MSNs was not significantly different in the dopamine-depleted network compared to control (z-score at 0 ms was 0.22 ± 0.03, $p = 0.18$). These results suggest that experimentally observed increases FS-D2 MSN connectivity could lead to aberrant synchrony of indirect-pathway striatal output.

Indeed, synchrony across D2 MSNs develops in a graded manner as a function of FS connectivity (Supplemental Fig. 4). Furthermore, synchrony in the model was highly influenced by changes in the strength of FS-MSN connections but only weakly affected by changes in the strength of MSN-MSN collaterals (Supplemental Fig. 5). Finally, a number of other changes that could affect synchrony have been observed in the striatum following dopamine depletion, including increases in MSN excitability and decreases in cortical inputs onto D2 MSNs (Azdad et al., 2009; Day et al., 2008). However, these parameters did not affect synchrony in our model as strongly as changes in FS-MSN connectivity (Supplemental Fig. 6).

Taken together, these results suggest that increased feedforward inhibition from FS interneurons onto D2 MSNs is sufficient to enhance synchrony, consistent with findings in other systems (Assisi et al., 2007; Atallah and Scanziani, 2009; Bartos et al., 2002; MacLeod and Laurent, 1996; Vida et al., 2006). By enhancing synchrony of D2 MSNs in the striatum, reorganization of FS microcircuits is predicted to strengthen indirect pathway regulation of downstream target nuclei, where MSN projections are highly convergent (Bolam et al., 2000; Smith et al., 1998). In this manner, changes in striatal microcircuits may contribute to the aberrant synchrony and amplification of pathological oscillations that emerge in the basal ganglia in PD.

Discussion

Dopamine is an important modulator of striatal function that dynamically regulates the basal ganglia circuit over short and long timescales. The rate and pattern of MSN activity in direct and indirect pathway circuits is regulated by a balance of excitation from cortical and thalamic inputs as well as inhibition from other MSNs and predominantly, FS interneurons. In this study, we show that dopamine depletion causes a target-specific reorganization of the feedforward inhibitory circuit through selective enhancement of FS connections to D2 MSNs. A simple model of the striatal microcircuit suggests that this pathway-specific increase in connectivity is sufficient to augment firing synchrony in indirect pathway projection neurons, thus potentially implicating reorganization of FS microcircuits in striatal dysfunction in Parkinson's disease.

Mechanisms that upregulate inhibition onto D2 MSNs

In the striatum of 6-OHDA-injected mice, we find that dopamine depletion causes an increase in FS innervation of D2 MSNs, driven by sprouting of FS axons. This was confirmed anatomically by reconstructions of FS interneurons and immunohistological analysis of presynaptic puncta, and functionally by paired recordings showing increased FS-D2 MSN connectivity and increased mIPSC frequency selectively onto D2 MSNs. These results are the first to demonstrate that dopamine depletion can induce a target-specific remodeling of FS innervations, which is both rapid (observed within 3 days) and persistent (observed at 4 weeks).

This target-specific plasticity may represent a homeostatic response to D2 MSN hyperactivity after dopamine depletion. Within hours to days after dopamine depletion, D2 MSNs show increased excitability (Fino et al., 2007; Mallet et al., 2006; Nicola et al., 2000), accompanied by reduced spine density (Day et al., 2006) and collaterals between both MSN subtypes (Taverna et al., 2008). The hyperactivity of MSNs in the indirect pathway could trigger compensatory upregulation of inhibition from FS interneurons, reminiscent of compensatory sprouting observed by some types of GABAergic interneurons in epilepsy (Bausch, 2005; Davenport et al., 1990; Klaassen et al., 2006; Palop et al., 2007). Indeed, previous studies have demonstrated that structural plasticity of GABAergic interneurons can occur within hours or days (Chen et al., 2011; Marik et al.).

The mechanisms of compensatory sprouting of inhibitory axons has long remained enigmatic (Valdes et al., 1982). In the hippocampus, a subset of inhibitory inputs are selectively strengthened by reductions in endocannabinoid (eCB) signaling (Kim and Alger, 2010), and in the striatum, reduced eCB-dependent LTD onto D2 MSNs is thought to contribute to increased drive on the indirect pathway following dopamine depletion (Kreitzer and Malenka, 2007). However, it does not appear that eCBs in the striatum contribute to compensatory sprouting of FS interneurons, because we did not observe changes in amplitude and short-term plasticity of IPSCs as described by (Kim and Alger, 2010). Alternatively, BDNF signaling through TrkB receptors has also been shown to regulate sprouting of inhibitory axons (Huang et al., 1999; Peng et al., 2010; Rutherford et al., 1997; Seil and Drake-Baumann, 2000; Swanwick et al., 2006), but changes in BDNF levels are not detected in striatum until 2 weeks after dopamine depletion, or not at all (Branchi et al.; Zhou et al., 1996).

The discovery of putative compensatory upregulation of inhibition onto D2 MSNs in response to dopamine depletion complements results that show increased inhibition onto D1 MSNs in response to elevated dopamine levels during chronic cocaine administration (Heiman et al., 2008), where hyperexcitability of D1 MSNs in the direct pathway is observed (Flores-Hernandez et al., 2002). Taken together, these results suggest that

feedforward inhibition in the striatum is dynamically regulated in a pathway-specific manner. Elevated levels of dopamine in the striatum lead to overactivity in the direct pathway, triggering compensatory increases in inhibition onto D1 MSNs, while diminished levels of dopamine in the striatum lead to overactivity in the indirect pathway, triggering compensatory increases in inhibition onto D2 MSNs.

Aberrant firing synchrony in the indirect pathway

It has long been hypothesized that motor deficits in PD patients result from overactivity of the indirect pathway relative to the direct pathway (Albin et al., 1989; DeLong, 1990). Recently, it was found that direct activation of D2 MSNs in the striatum alone is sufficient to suppress movement and that motor deficits in mice rendered parkinsonian with 6-OHDA could be partially restored by direct activation of D1 MSNs (Kravitz et al., 2010). These results demonstrate that changes in the relative activity of D1 and D2 MSNs in the striatum can lead to widespread dysfunction throughout the basal ganglia.

Increases in feedforward inhibition onto overactive D2 MSNs in dopamine-depleted striatum would seemingly counteract excess activity in this pathway. However, this homeostatic response could paradoxically amplify indirect-pathway output by synchronizing activity of D2 MSNs across the striatum. FS interneurons are well described mediators of neuronal synchrony whose divergent innervation of target neurons and synaptic properties shape the output patterns of a network (Bartos et al., 2007; Cobb et al., 1995; Gabernet et al., 2005; Pouille et al., 2009; Pouille and Scanziani, 2001; Tamas et al., 2000). The ability of feedforward inhibition to synchronize the activity of large populations of neurons has been shown both computationally (Assisi et al., 2007; Bartos et al., 2002; MacLeod and Laurent, 1996; Vida et al., 2006) and experimentally (Fuchs et al., 2007; Sohal et al., 2009). However, it is important to point out that FS interneurons may function differently in the striatum than in other brain regions (Gage et al., 2010), and a more detailed study of FS inhibition under control conditions and after dopamine depletion (including analysis of GABA reversal potential and KCC2 expression) would be revealing.

High convergence of striatal outputs onto neurons in downstream nuclei (Smith et al., 1998) suggest that some degree of synchronization across groups of MSNs is required to propagate information (Courtemanche et al., 2003; Graybiel et al., 1994). However, synchrony across large populations of MSNs is rarely seen in healthy individuals and rather, is a hallmark of striatal dysfunction in motor diseases such as PD and dystonia (Buzsaki et al., 1990; Costa et al., 2006; Gernert et al., 2002; Hammond et al., 2007; Hutchison et al., 2004; Kuhn et al., 2008). In particular, dopamine depletion is associated with increased network oscillations in the β-frequency band which may occlude normal signal propagation through the basal ganglia (Brown, 2003; Kuhn et al., 2004; Mallet et al., 2008b).

Although pathological β-oscillations after dopamine depletion are a feature of the entire basal ganglia network, some of the most striking shifts in neuronal firing patterns occur in the globus pallidus (GP) and subthalamic nucleus (STN) (Bevan et al., 2002; Mallet et al., 2008a; Terman et al., 2002). These nuclei become highly coupled in an oscillatory pattern after dopamine depletion and disruption of this abnormal synchrony with deep brain stimulation is an effective therapeutic treatment in patients with PD (Bevan et al., 2002; Hammond et al., 2007). Although GP neurons do not show a substantial change in average firing rate after dopamine depletion, they do show changes in firing pattern, shifting to a synchronized, bursting mode of firing in resting animals or PD patients (Brown et al., 2001; Raz et al., 2000). In part, this altered firing pattern may depend on increased synchronous inhibition from striatal D2 MSNs (Terman et al., 2002). However, a number of other changes in the striatum have been described after dopamine depletion that could alter the output of D2 MSNs. These include changes in LTD and LTP at excitatory inputs onto MSNs

(Calabresi et al., 2007; Kreitzer and Malenka, 2008; Lovinger, 2010; Shen et al., 2008), decreased spine density and loss of glutamatergic synapses onto D2 MSNs (Day et al., 2008), changes in cholinergic signaling (Ding et al., 2006), and changes in a non-FS population of GABAergic interneurons (Dehorter et al., 2009).

In this study, we use a simple model of the striatal circuit to demonstrate that experimentally increased innervation of D2 MSNs by FS interneurons may be sufficient to enhance synchrony of D2 MSNs. This, along with other changes in striatal circuitry, could enhance D2 MSN regulation of downstream target neurons and contribute to increased synchrony in the GP and the STN (Burkhardt et al., 2007; Costa et al., 2006; Terman et al., 2002; Walters et al., 2007). Furthermore, because a subset of GP neurons project back to striatal interneurons (Bevan et al., 1998; Gage et al.), this may also amplify indirect-pathway synchrony in the striatum, leading to robust pathological oscillations in the indirect-pathway basal ganglia circuit.

Experimental Procedures

Electrophysiological recordings

Coronal sections containing dorsal striatum were prepared in cold sucrose cutting solution (in mM): 79 NaCl, 23 $NaHCO_3$, 68 sucrose, 12 glucose, 2.3 KCl, 1.1 NaH_2PO_4, 6 $MgCl_2$, and 0.5 $CaCl_2$. Slices were transferred to a chamber filled with warmed carbogenated ACSF containing (in mM): 125 NaCl, 26 $NaHCO_3$, 2.5 KCl, 1 $MgCl_2$, 2 $CaCl_2$, 1.25 NaH_2PO_4, and 12.5 glucose and were incubated at 31 – 33°C for 30 minutes, then allowed to recover at room temperature for an additional 30 minutes before recording.

Internal solutions were either K-based, for current clamp recordings from FS interneurons in paired experiments (in mM): 130 $KMeSO_3$, 10 NaCl, 2 $MgCl_2$, 0.16 $CaCl_2$, 0.5 EGTA, 10 Hepes, 2 Mg-ATP, 0.3 Na-GTP, pH 7.25 or Cs-based, for all voltage clamp recordings (in mM): 120 CsCl, 15 $CsMeSO_3$, 8 NaCl, 0.5 EGTA, 10 Hepes, 2 Mg-ATP, 0.3 Na-GTP, 5 QX-314, pH 7.3. All recordings were performed at 31 – 33°C in ACSF (see above). For experiments measuring mIPSCs, 1 μM TTX (Ascent) and 5 μM NBQX (Ascent) were added to the external. For experiments using dopamine antagonists, 5 μM SCH23390 (Tocris) and 10 μM sulpiride (Tocris) were added to the external saline.

Dopamine depletions

Mice were pretreated with desipramine (25mg/kg, Sigma) and unilaterally injected with 6-OHDA at 3–4 weeks of age. Experiments were typically performed 3–7 days after 6-OHDA injections unless otherwise noted. All changes observed in FS microcircuits at 1 week were already present at 3 days, so data from these time points were pooled. Due to previous reports of changes in contralateral striatum following unilateral 6-OHDA injections, saline-injected mice were used as controls (Schwarting and Huston, 1996b).

Histology and immunostaining

TH immunostains were performed on 30 μm sections, resectioned from acute slices (250–300 μm thick) used for recording. Immunostains for PV and vGAT were performed on 30 μm sections prepared from fixed brains of D2-GFP mice. To quantify overall colocalization between vGAT and PV, images were imported into ImageJ, where intensity thresholds and Manders overlap coefficients were determined by JACoP (Bolte and Cordelieres, 2006). Biocytin cell fills were performed on FS interneurons recorded in the striatum from 300 μm-thick coronal slices. Slices were fixed 30 min − 2 hours after filling a neuron in 4% PFA overnight at 4°C.

Statistics

Throughout the paper, t-tests for unpaired data were used to test for significance unless otherwise noted. The nonparametric Wilcoxon signed rank test was used when data were not normally distributed. A Chi-square test with Yate's correction was used to test for significance of FS-D1 MSN and FS-D2 MSN connectivities.

Computational model

Our model of feedforward inhibition in the striatum was adapted from one used by (Atallah and Scanziani, 2009). Each cell was modeled as a single compartment, integrate-and-fire neuron. Spiking activity for individual cells was initiated by independent stochastic background synaptic activity (Gaussian noise with a standard deviation of 100 pA). The networks contained 20 FS interneurons, 400 D1 MSNs and 400 D2 MSNs, matching observations that FS interneurons comprise ~2% of all striatal neurons (Gittis et al., 2010; Tepper et al., 2004). Intrinsic parameters of model striatal neurons were based on experimentally measured values (Gittis et al., 2010; Kreitzer and Malenka, 2007) and tuned to produce realistic firing rates measured *in vivo* (Berke et al., 2004; Gage et al., 2010). As observed experimentally, individual FS interneurons made synaptic projections onto D1 and D2 MSNs as well as other FS interneurons (Gittis et al., 2010; Planert et al., 2010); MSNs make synaptic projections to other MSNs (Planert et al., 2010; Taverna et al., 2008) and these lateral connections were also included in the model. For the population cross-correlogram (1500 pairs), data was rebinned at 1 ms.To normalize across cell pairs, z-score was calculated for each individual correlogram.

$$z - score = \frac{x - \mu}{\sigma}$$

Where x is the spikes/bin in the individual cross-correlogram, μ is the mean of x and σ is the standard deviation of x.

Supplementary Material

Refer to Web version on PubMed Central for supplementary material.

Acknowledgments

The authors are grateful to K. Bender, J. Fish, and P. Ohara for assistance with cell fills and neuron reconstructions. Thank you to R. Johnson in the Vanderbilt Neurochemistry Core for performing HPLC analyses and K. Thorn and A. Thwin in the UCSF Nikon imaging center for assistance with microscopy. Mini analysis and data acquisition routines for Igor Pro were written by M.A. Xu-Friedman. This work was supported by grants to AG from the Tourette Syndrome Association and NIH grant F32 NS065641, and to AK by NIH grant R01 NS064984, the Pew Biomedical Scholars Program, the W.M. Keck Foundation, and the McKnight Foundation.

References

Albin RL, Young AB, Penney JB. The functional anatomy of basal ganglia disorders. Trends Neurosci. 1989; 12:366–375. [PubMed: 2479133]

Assisi C, Stopfer M, Laurent G, Bazhenov M. Adaptive regulation of sparseness by feedforward inhibition. Nat Neurosci. 2007; 10:1176–1184. [PubMed: 17660812]

Atallah BV, Scanziani M. Instantaneous modulation of gamma oscillation frequency by balancing excitation with inhibition. Neuron. 2009; 62:566–577. [PubMed: 19477157]

Azdad K, Chavez M, Don Bischop P, Wetzelaer P, Marescau B, De Deyn PP, Gall D, Schiffmann SN. Homeostatic plasticity of striatal neurons intrinsic excitability following dopamine depletion. PLoS One. 2009; 4 e6908.

Bacci A, Rudolph U, Huguenard JR, Prince DA. Major differences in inhibitory synaptic transmission onto two neocortical interneuron subclasses. J Neurosci. 2003; 23:9664–9674. [PubMed: 14573546]

Bartos M, Vida I, Frotscher M, Meyer A, Monyer H, Geiger JR, Jonas P. Fast synaptic inhibition promotes synchronized gamma oscillations in hippocampal interneuron networks. Proc Natl Acad Sci U S A. 2002; 99:13222–13227. [PubMed: 12235359]

Bartos M, Vida I, Jonas P. Synaptic mechanisms of synchronized gamma oscillations in inhibitory interneuron networks. Nat Rev Neurosci. 2007; 8:45–56. [PubMed: 17180162]

Bausch SB. Axonal sprouting of GABAergic interneurons in temporal lobe epilepsy. Epilepsy Behav. 2005; 7:390–400. [PubMed: 16198153]

Berke JD, Okatan M, Skurski J, Eichenbaum HB. Oscillatory entrainment of striatal neurons in freely moving rats. Neuron. 2004; 43:883–896. [PubMed: 15363398]

Bevan MD, Booth PA, Eaton SA, Bolam JP. Selective innervation of neostriatal interneurons by a subclass of neuron in the globus pallidus of the rat. J Neurosci. 1998; 18:9438–9452. [PubMed: 9801382]

Bevan MD, Magill PJ, Terman D, Bolam JP, Wilson CJ. Move to the rhythm: oscillations in the subthalamic nucleus-external globus pallidus network. Trends Neurosci. 2002; 25:525–531. [PubMed: 12220881]

Bolam JP, Hanley JJ, Booth PA, Bevan MD. Synaptic organisation of the basal ganglia. J Anat. 2000; 196(Pt 4):527–542. [PubMed: 10923985]

Bolte S, Cordelieres FP. A guided tour into subcellular colocalization analysis in light microscopy. J Microsc. 2006; 224:213–232. [PubMed: 17210054]

Bracci E, Centonze D, Bernardi G, Calabresi P. Dopamine excites fast-spiking interneurons in the striatum. J Neurophysiol. 2002; 87:2190–2194. [PubMed: 11929936]

Branchi I, D'Andrea I, Armida M, Carnevale D, Ajmone-Cat MA, Pezzola A, Potenza RL, Morgese MG, Cassano T, Minghetti L, et al. Striatal 6-OHDA lesion in mice: Investigating early neurochemical changes underlying Parkinson's disease. Behav Brain Res. 2009; 208:137–143. [PubMed: 19914295]

Brown P. Oscillatory nature of human basal ganglia activity: relationship to the pathophysiology of Parkinson's disease. Mov Disord. 2003; 18:357–363. [PubMed: 12671940]

Brown P, Oliviero A, Mazzone P, Insola A, Tonali P, Di Lazzaro V. Dopamine dependency of oscillations between subthalamic nucleus and pallidum in Parkinson's disease. J Neurosci. 2001; 21:1033–1038. [PubMed: 11157088]

Burkhardt JM, Constantinidis C, Anstrom KK, Roberts DC, Woodward DJ. Synchronous oscillations and phase reorganization in the basal ganglia during akinesia induced by high-dose haloperidol. Eur J Neurosci. 2007; 26:1912–1924. [PubMed: 17897397]

Buzsaki G, Smith A, Berger S, Fisher LJ, Gage FH. Petit mal epilepsy and parkinsonian tremor: hypothesis of a common pacemaker. Neuroscience. 1990; 36:1–14. [PubMed: 2120612]

Calabresi P, Picconi B, Tozzi A, Di Filippo M. Dopamine-mediated regulation of corticostriatal synaptic plasticity. Trends Neurosci. 2007; 30:211–219. [PubMed: 17367873]

Centonze D, Grande C, Usiello A, Gubellini P, Erbs E, Martin AB, Pisani A, Tognazzi N, Bernardi G, Moratalla R, et al. Receptor subtypes involved in the presynaptic and postsynaptic actions of dopamine on striatal interneurons. J Neurosci. 2003; 23:6245–6254. [PubMed: 12867509]

Chen JL, Lin WC, Cha JW, So PT, Kubota Y, Nedivi E. Structural basis for the role of inhibition in facilitating adult brain plasticity. Nat Neurosci. 2011; 14:587–594. [PubMed: 21478885]

Cobb SR, Buhl EH, Halasy K, Paulsen O, Somogyi P. Synchronization of neuronal activity in hippocampus by individual GABAergic interneurons. Nature. 1995; 378:75–78. [PubMed: 7477292]

Costa RM, Lin SC, Sotnikova TD, Cyr M, Gainetdinov RR, Caron MG, Nicolelis MA. Rapid alterations in corticostriatal ensemble coordination during acute dopamine-dependent motor dysfunction. Neuron. 2006; 52:359–369. [PubMed: 17046697]

Courtemanche R, Fujii N, Graybiel AM. Synchronous, focally modulated beta-band oscillations characterize local field potential activity in the striatum of awake behaving monkeys. J Neurosci. 2003; 23:11741–11752. [PubMed: 14684876]

Davenport CJ, Brown WJ, Babb TL. Sprouting of GABAergic and mossy fiber axons in dentate gyrus following intrahippocampal kainate in the rat. Exp Neurol. 1990; 109:180–190. [PubMed: 1696207]

Day M, Wang Z, Ding J, An X, Ingham CA, Shering AF, Wokosin D, Ilijic E, Sun Z, Sampson AR, et al. Selective elimination of glutamatergic synapses on striatopallidal neurons in Parkinson disease models. Nat Neurosci. 2006; 9:251–259. [PubMed: 16415865]

Day M, Wokosin D, Plotkin JL, Tian X, Surmeier DJ. Differential excitability and modulation of striatal medium spiny neuron dendrites. J Neurosci. 2008; 28:11603–11614. [PubMed: 18987196]

Dehorter N, Guigoni C, Lopez C, Hirsch J, Eusebio A, Ben-Ari Y, Hammond C. Dopamine-deprived striatal GABAergic interneurons burst and generate repetitive gigantic IPSCs in medium spiny neurons. J Neurosci. 2009; 29:7776–7787. [PubMed: 19535589]

DeLong MR. Primate models of movement disorders of basal ganglia origin. Trends Neurosci. 1990; 13:281–285. [PubMed: 1695404]

Ding J, Guzman JN, Tkatch T, Chen S, Goldberg JA, Ebert PJ, Levitt P, Wilson CJ, Hamm HE, Surmeier DJ. RGS4-dependent attenuation of M4 autoreceptor function in striatal cholinergic interneurons following dopamine depletion. Nat Neurosci. 2006; 9:832–842. [PubMed: 16699510]

Fino E, Glowinski J, Venance L. Effects of acute dopamine depletion on the electrophysiological properties of striatal neurons. Neurosci Res. 2007; 58:305–316. [PubMed: 17499375]

Flores-Hernandez J, Cepeda C, Hernandez-Echeagaray E, Calvert CR, Jokel ES, Fienberg AA, Greengard P, Levine MS. Dopamine enhancement of NMDA currents in dissociated medium-sized striatal neurons: role of D1 receptors and DARPP-32. J Neurophysiol. 2002; 88:3010–3020. [PubMed: 12466426]

Foldy C, Lee SY, Szabadics J, Neu A, Soltesz I. Cell type-specific gating of perisomatic inhibition by cholecystokinin. Nat Neurosci. 2007; 10:1128–1130. [PubMed: 17676058]

Fuchs EC, Zivkovic AR, Cunningham MO, Middleton S, Lebeau FE, Bannerman DM, Rozov A, Whittington MA, Traub RD, Rawlins JN, Monyer H. Recruitment of parvalbumin-positive interneurons determines hippocampal function and associated behavior. Neuron. 2007; 53:591–604. [PubMed: 17296559]

Gabernet L, Jadhav SP, Feldman DE, Carandini M, Scanziani M. Somatosensory integration controlled by dynamic thalamocortical feed-forward inhibition. Neuron. 2005; 48:315–327. [PubMed: 16242411]

Gage GJ, Stoetzner CR, Wiltschko AB, Berke JD. Selective Activation of Striatal Fast-Spiking Interneurons during Choice Execution. Neuron. 2010; 67:466–479. [PubMed: 20696383]

Galvan A, Wichmann T. GABAergic circuits in the basal ganglia and movement disorders. Prog Brain Res. 2007; 160:287–312. [PubMed: 17499121]

Gernert M, Bennay M, Fedrowitz M, Rehders JH, Richter A. Altered discharge pattern of basal ganglia output neurons in an animal model of idiopathic dystonia. J Neurosci. 2002; 22:7244–7253. [PubMed: 12177219]

Gertler TS, Chan CS, Surmeier DJ. Dichotomous anatomical properties of adult striatal medium spiny neurons. J Neurosci. 2008; 28:10814–10824. [PubMed: 18945889]

Gittis AH, Nelson AB, Thwin MT, Palop JJ, Kreitzer AC. Distinct roles of GABAergic interneurons in the regulation of striatal output pathways. J Neurosci. 2010; 30:2223–2234. [PubMed: 20147549]

Graybiel AM, Aosaki T, Flaherty AW, Kimura M. The basal ganglia and adaptive motor control. Science. 1994; 265:1826–1831. [PubMed: 8091209]

Hammond C, Bergman H, Brown P. Pathological synchronization in Parkinson's disease: networks, models and treatments. Trends Neurosci. 2007; 30:357–364. [PubMed: 17532060]

Heiman M, Schaefer A, Gong S, Peterson JD, Day M, Ramsey KE, Suarez-Farinas M, Schwarz C, Stephan DA, Surmeier DJ, et al. A translational profiling approach for the molecular characterization of CNS cell types. Cell. 2008; 135:738–748. [PubMed: 19013281]

Huang ZJ, Kirkwood A, Pizzorusso T, Porciatti V, Morales B, Bear MF, Maffei L, Tonegawa S. BDNF regulates the maturation of inhibition and the critical period of plasticity in mouse visual cortex. Cell. 1999; 98:739–755. [PubMed: 10499792]

Hutchison WD, Dostrovsky JO, Walters JR, Courtemanche R, Boraud T, Goldberg J, Brown P. Neuronal oscillations in the basal ganglia and movement disorders: evidence from whole animal and human recordings. J Neurosci. 2004; 24:9240–9243. [PubMed: 15496658]

Jaidar O, Carrillo-Reid L, Hernandez A, Drucker-Colin R, Bargas J, Hernandez-Cruz A. Dynamics of the parkinsonian striatal microcircuit: entrainment into a dominant network state. J Neurosci. 2010; 30:11326–11336. [PubMed: 20739553]

Kawaguchi Y. Physiological, morphological, and histochemical characterization of three classes of interneurons in rat neostriatum. J Neurosci. 1993; 13:4908–4923. [PubMed: 7693897]

Kawaguchi Y, Wilson CJ, Augood SJ, Emson PC. Striatal interneurones: chemical, physiological and morphological characterization. Trends Neurosci. 1995; 18:527–535. [PubMed: 8638293]

Kim J, Alger BE. Reduction in endocannabinoid tone is a homeostatic mechanism for specific inhibitory synapses. Nat Neurosci. 2010; 13:592–600. [PubMed: 20348918]

Klaassen A, Glykys J, Maguire J, Labarca C, Mody I, Boulter J. Seizures and enhanced cortical GABAergic inhibition in two mouse models of human autosomal dominant nocturnal frontal lobe epilepsy. Proc Natl Acad Sci U S A. 2006; 103:19152–19157. [PubMed: 17146052]

Koos T, Tepper JM, Wilson CJ. Comparison of IPSCs evoked by spiny and fast-spiking neurons in the neostriatum. J Neurosci. 2004; 24:7916–7922. [PubMed: 15356204]

Kravitz AV, Freeze BS, Parker PR, Kay K, Thwin MT, Deisseroth K, Kreitzer AC. Regulation of parkinsonian motor behaviours by optogenetic control of basal ganglia circuitry. Nature. 2010; 466:622–626. [PubMed: 20613723]

Kreitzer AC. Physiology and pharmacology of striatal neurons. Annu Rev Neurosci. 2009; 32:127–147. [PubMed: 19400717]

Kreitzer AC, Malenka RC. Endocannabinoid-mediated rescue of striatal LTD and motor deficits in Parkinson's disease models. Nature. 2007; 445:643–647. [PubMed: 17287809]

Kreitzer AC, Malenka RC. Striatal plasticity and basal ganglia circuit function. Neuron. 2008; 60:543–554. [PubMed: 19038213]

Kuhn AA, Brucke C, Schneider GH, Trottenberg T, Kivi A, Kupsch A, Capelle HH, Krauss JK, Brown P. Increased beta activity in dystonia patients after drug-induced dopamine deficiency. Exp Neurol. 2008; 214:140–143. [PubMed: 18760276]

Kuhn AA, Williams D, Kupsch A, Limousin P, Hariz M, Schneider GH, Yarrow K, Brown P. Event-related beta desynchronization in human subthalamic nucleus correlates with motor performance. Brain. 2004; 127:735–746. [PubMed: 14960502]

Lovinger DM. Neurotransmitter roles in synaptic modulation, plasticity and learning in the dorsal striatum. Neuropharmacology. 2010; 58:951–961. [PubMed: 20096294]

MacLeod K, Laurent G. Distinct mechanisms for synchronization and temporal patterning of odor-encoding neural assemblies. Science. 1996; 274:976–979. [PubMed: 8875938]

Mallet N, Ballion B, Le Moine C, Gonon F. Cortical inputs and GABA interneurons imbalance projection neurons in the striatum of parkinsonian rats. J Neurosci. 2006; 26:3875–3884. [PubMed: 16597742]

Mallet N, Pogosyan A, Marton LF, Bolam JP, Brown P, Magill PJ. Parkinsonian beta oscillations in the external globus pallidus and their relationship with subthalamic nucleus activity. J Neurosci. 2008a; 28:14245–14258. [PubMed: 19109506]

Mallet N, Pogosyan A, Sharott A, Csicsvari J, Bolam JP, Brown P, Magill PJ. Disrupted dopamine transmission and the emergence of exaggerated beta oscillations in subthalamic nucleus and cerebral cortex. J Neurosci. 2008b; 28:4795–4806. [PubMed: 18448656]

Marik SA, Yamahachi H, McManus JN, Szabo G, Gilbert CD. Axonal dynamics of excitatory and inhibitory neurons in somatosensory cortex. PLoS Biol. 8 e1000395.

Matamales M, Bertran-Gonzalez J, Salomon L, Degos B, Deniau JM, Valjent E, Herve D, Girault JA. Striatal medium-sized spiny neurons: identification by nuclear staining and study of neuronal subpopulations in BAC transgenic mice. PLoS One. 2009; 4 e4770.

Nicola SM, Surmeier J, Malenka RC. Dopaminergic modulation of neuronal excitability in the striatum and nucleus accumbens. Annu Rev Neurosci. 2000; 23:185–215. [PubMed: 10845063]

Palop JJ, Chin J, Roberson ED, Wang J, Thwin MT, Bien-Ly N, Yoo J, Ho KO, Yu GQ, Kreitzer A, et al. Aberrant excitatory neuronal activity and compensatory remodeling of inhibitory hippocampal circuits in mouse models of Alzheimer's disease. Neuron. 2007; 55:697–711. [PubMed: 17785178]

Peng YR, Zeng SY, Song HL, Li MY, Yamada MK, Yu X. Postsynaptic spiking homeostatically induces cell-autonomous regulation of inhibitory inputs via retrograde signaling. J Neurosci. 2010; 30:16220–16231. [PubMed: 21123568]

Planert H, Szydlowski SN, Hjorth JJ, Grillner S, Silberberg G. Dynamics of synaptic transmission between fast-spiking interneurons and striatal projection neurons of the direct and indirect pathways. J Neurosci. 2010; 30:3499–3507. [PubMed: 20203210]

Pouille F, Marin-Burgin A, Adesnik H, Atallah BV, Scanziani M. Input normalization by global feedforward inhibition expands cortical dynamic range. Nat Neurosci. 2009; 12:1577–1585. [PubMed: 19881502]

Pouille F, Scanziani M. Enforcement of temporal fidelity in pyramidal cells by somatic feed-forward inhibition. Science. 2001; 293:1159–1163. [PubMed: 11498596]

Raz A, Vaadia E, Bergman H. Firing patterns and correlations of spontaneous discharge of pallidal neurons in the normal and the tremulous 1-methyl-4-phenyl-1,2,3,6-tetrahydropyridine vervet model of parkinsonism. J Neurosci. 2000; 20:8559–8571. [PubMed: 11069964]

Rutherford LC, DeWan A, Lauer HM, Turrigiano GG. Brain-derived neurotrophic factor mediates the activity-dependent regulation of inhibition in neocortical cultures. J Neurosci. 1997; 17:4527–4535. [PubMed: 9169513]

Schwarting RK, Huston JP. The unilateral 6-hydroxydopamine lesion model in behavioral brain research. Analysis of functional deficits, recovery and treatments. Prog Neurobiol. 1996a; 50:275–331. [PubMed: 8971983]

Schwarting RK, Huston JP. Unilateral 6-hydroxydopamine lesions of meso-striatal dopamine neurons and their physiological sequelae. Prog Neurobiol. 1996b; 49:215–266. [PubMed: 8878304]

Seil FJ, Drake-Baumann R. TrkB receptor ligands promote activity-dependent inhibitory synaptogenesis. J Neurosci. 2000; 20:5367–5373. [PubMed: 10884321]

Shen W, Flajolet M, Greengard P, Surmeier DJ. Dichotomous dopaminergic control of striatal synaptic plasticity. Science. 2008; 321:848–851. [PubMed: 18687967]

Shuen JA, Chen M, Gloss B, Calakos N. Drd1a-tdTomato BAC transgenic mice for simultaneous visualization of medium spiny neurons in the direct and indirect pathways of the basal ganglia. J Neurosci. 2008; 28:2681–2685. [PubMed: 18337395]

Smith Y, Bevan MD, Shink E, Bolam JP. Microcircuitry of the direct and indirect pathways of the basal ganglia. Neuroscience. 1998; 86:353–387. [PubMed: 9881853]

Sohal VS, Zhang F, Yizhar O, Deisseroth K. Parvalbumin neurons and gamma rhythms enhance cortical circuit performance. Nature. 2009; 459:698–702. [PubMed: 19396159]

Suzuki N, Bekkers JM. Distinctive classes of GABAergic interneurons provide layer-specific phasic inhibition in the anterior piriform cortex. Cereb Cortex. 2010; 20:2971–2984. [PubMed: 20457693]

Swanwick CC, Murthy NR, Kapur J. Activity-dependent scaling of GABAergic synapse strength is regulated by brain-derived neurotrophic factor. Mol Cell Neurosci. 2006; 31:481–492. [PubMed: 16330218]

Tamas G, Buhl EH, Lorincz A, Somogyi P. Proximally targeted GABAergic synapses and gap junctions synchronize cortical interneurons. Nat Neurosci. 2000; 3:366–371. [PubMed: 10725926]

Taverna S, Ilijic E, Surmeier DJ. Recurrent collateral connections of striatal medium spiny neurons are disrupted in models of Parkinson's disease. J Neurosci. 2008; 28:5504–5512. [PubMed: 18495884]

Tepper JM, Koos T, Wilson CJ. GABAergic microcircuits in the neostriatum. Trends Neurosci. 2004; 27:662–669. [PubMed: 15474166]

Terman D, Rubin JE, Yew AC, Wilson CJ. Activity patterns in a model for the subthalamopallidal network of the basal ganglia. J Neurosci. 2002; 22:2963–2976. [PubMed: 11923461]

Valdes F, Dasheiff RM, Birmingham F, Crutcher KA, McNamara JO. Benzodiazepine receptor increases after repeated seizures: evidence for localization to dentate granule cells. Proc Natl Acad Sci U S A. 1982; 79:193–197. [PubMed: 6275387]

Varga C, Lee SY, Soltesz I. Target-selective GABAergic control of entorhinal cortex output. Nat Neurosci. 2010; 13:822–824. [PubMed: 20512133]

Vida I, Bartos M, Jonas P. Shunting inhibition improves robustness of gamma oscillations in hippocampal interneuron networks by homogenizing firing rates. Neuron. 2006; 49:107–117. [PubMed: 16387643]

Walters JR, Hu D, Itoga CA, Parr-Brownlie LC, Bergstrom DA. Phase relationships support a role for coordinated activity in the indirect pathway in organizing slow oscillations in basal ganglia output after loss of dopamine. Neuroscience. 2007; 144:762–776. [PubMed: 17112675]

Xiang Z, Huguenard JR, Prince DA. Synaptic inhibition of pyramidal cells evoked by different interneuronal subtypes in layer v of rat visual cortex. J Neurophysiol. 2002; 88:740–750. [PubMed: 12163526]

Zhou J, Pliego-Rivero B, Bradford HF, Stern GM. The BDNF content of postnatal and adult rat brain: the effects of 6-hydroxydopamine lesions in adult brain. Brain Res Dev Brain Res. 1996; 97:297–303.

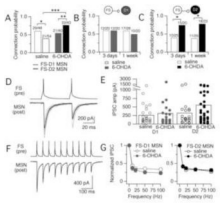

Figure 1. Changes in FS-MSNs connections after dopamine depletion

A. Probabilities of finding synaptic connections between presynaptic FS interneurons and postsynaptic D1 and D2 MSNs in striatum of saline- or 6-OHDA-injected mice. The number of connections per number of attempts is listed for each condition. In saline-injected mice, FS interneurons were more likely to be connected to D1 MSNs compared to D2 MSNs ($p = 0.05$) but in 6-OHDA-injected mice, FS interneurons were more likely to be connected to D2 MSNs compared to D1 MSNs ($p = 0.04$). *$p = 0.05$, **$p = 0.04$, ***$p = 0.004$. **B.** Probabilities of finding synaptic connections for FS-D1 MSN pairs either 3 days or 1 week after surgeries. Connection probability was not significantly different at either time point. **C.** Same as (B) but for FS-D2 MSN pairs. At both 3 days and 1 week after 6-OHDA injection, the probabilities of finding synaptic connections onto D2 MSNs were significantly increased compared to those measured in saline-injected mice (*$p = 0.04$ at 3 days and 0.009 at 1 week). **D.** Example of a paired recording where action potentials in a presynaptic FS interneuron elicit uIPSCs in a postsynaptic MSN. Individual trials (n = 10) are shown in grey with the average overlaid in black. The example is a recording from a 6-OHDA-injected mouse and the postsynaptic cell is a D1 MSN. **E.** Amplitudes of uIPSCs recorded in D1 and D2 MSNs in saline- and 6-OHDA-injected mice. There was no significant difference in uIPSC amplitudes across conditions. Circles represent data from individual cells and bars are the average for each population ($saline_{D1} = 267 \pm 273$ pA; $saline_{D2} = 328 \pm 406$ pA; $6\text{-}OHDA_{D1} = 322 \pm 470$ pA; $6\text{-}OHDA_{D2} = 566 \pm 781$ pA). **F.** Example of a paired recording in which a train of 10 action potentials (20 Hz) in a presynaptic FS interneuron elicits uIPSCs in a postsynaptic MSN. The example is a recording from a 6-OHDA injected mouse and the postsynaptic cell is a D2 MSN. **G.** Synaptic depression of FS-MSN synapses measured at 10, 20, 50, and 100 Hz in saline- and 6-OHDA-injected mice. Synaptic depression was calculated as the amplitude of $uIPSC_{8–10}$ / $uIPSC_1$. Error bars are sem. Synaptic depression was similar onto D1 (n = 9, saline; n = 9, 6-OHDA) and D2 MSNs (n = 8 saline; n = 8, 6-OHDA)) and was not changed by dopamine depletion.

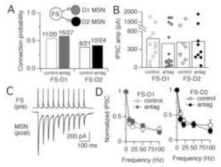

Figure 2. FS-MSN synapses are not silenced by tonic dopamine levels in the slice

A. Bar graph comparing the probability of finding synaptic connections between presynaptic FS interneurons and postsynaptic D1 or D2 MSNs in control slices vs. slices incubated in a cocktail of D1 and D2 dopamine receptor antagonists (5 μM SCH23390 and 10 μM sulpiride, respectively). **B.** Amplitudes of uIPSCs recorded in D1 and D2 MSNs in control slices and from slices perfused with dopamine receptor antagonists. There was no significant difference in uIPSC amplitudes across conditions. Circles represent data from individual cells and bars are the average for each populations. **C.** Example of a paired recording in which a train of 10 action potentials (20 Hz) in a presynaptic FS interneuron elicits uIPSCs in a postsynaptic MSN. The example is from a recording done in the presence of dopamine receptor antagonists. The postsynaptic cell is a D1 MSN. **D.** Synaptic depression of FS-MSN synapses measured at 10, 20, 50, and 100 Hz in control slices and slices perfused with dopamine receptor antagonists. Synaptic depression was calculated as the amplitude of $uIPSC_{8–10}$ / $uIPSC_1$. Error bars are sem. Synaptic depression was similar onto D1 and D2 MSNs and was not changed by application of dopamine receptor antagonists.

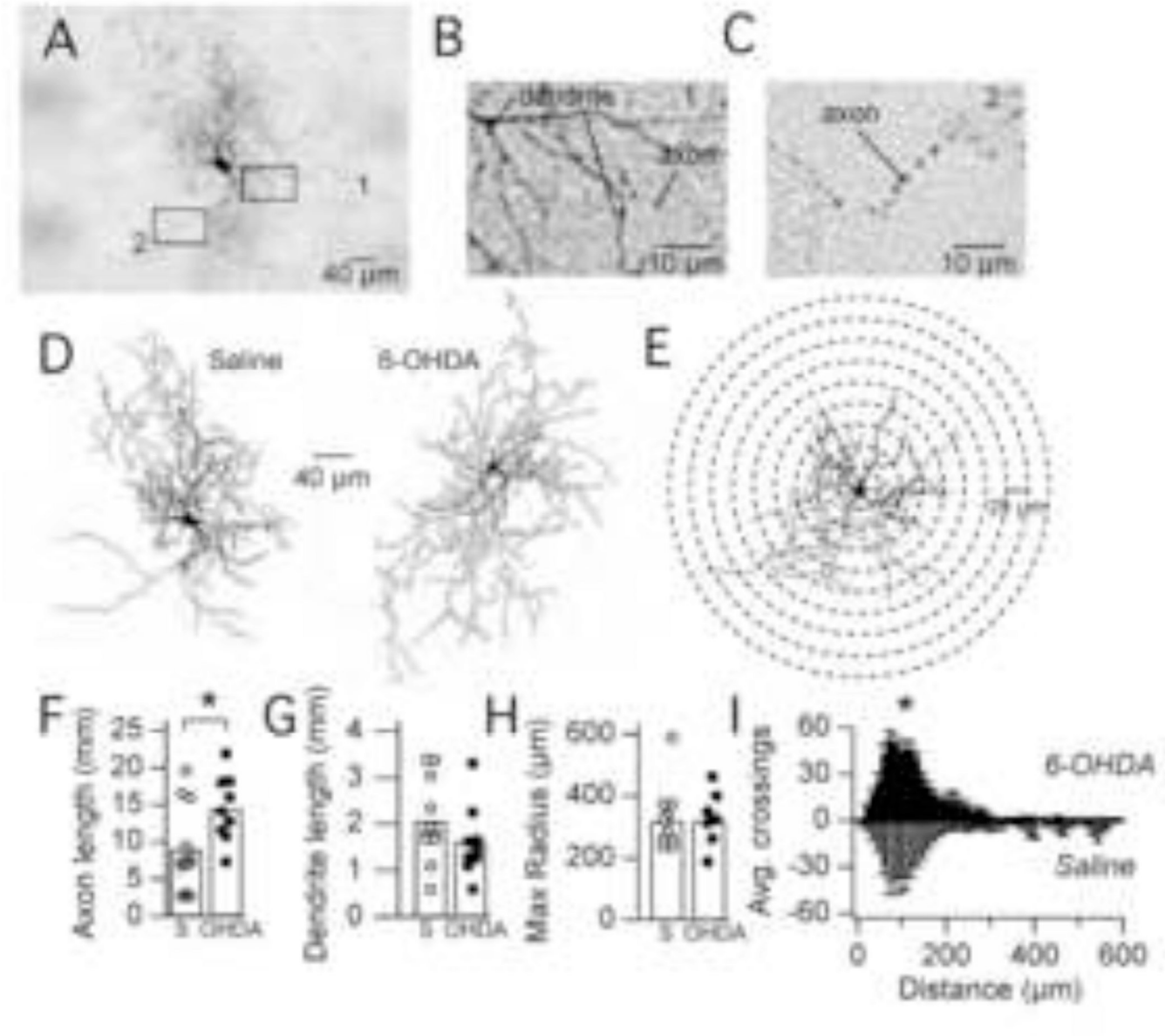

Figure 3. Anatomical changes in FS interneurons after dopamine depletion

A. Brightfield image of a biocytin-filled FS interneuron from a saline-injected mouse. **B–C.** Higher magnification images of axons and dendrites for the boxed regions '1' and '2' in A. Axons were distinguished from dendrites based on their narrower diameter and beaded appearance. **D.** Reconstructions of biocytin-filled FS interneurons from the striatum of saline-injected (*left, same cell as in A*) or 6-OHDA-injected (*right*) mice. Axons are grey and dendrites are black. **E.** Example of a reconstructed neuron (from a saline-injected mouse) within the radial grid used for a Sholl analysis. For display purposes, every other circle is omitted, so radii increase in 25 µm intervals. For the actual analysis, radii increased in 12.5 µm intervals. **F.** Bar graph showing significant increase (*p = 0.04) in total axon length of FS interneurons in 6-OHDA-injected mice relative to saline-injected mice. **G.** Bar graph showing no significant change in total dendrite length of FS interneurons in 6-OHDA-injected mice relative to saline-injected mice. **H.** Bar graph displaying the maximum radius at which axon crossings were detected. The maximum radius (a measure of axonal area) was

not significantly different between saline- and 6-OHDA-injected mice. **I.** Graph showing the average number of grid crossings as a function of distance from the soma by axons of FS interneurons in saline-injected and 6-OHDA-injected mice. The number of crossings was significantly greater in 6-OHDA-injected mice compared to saline-injected mice (*p = 0.04).

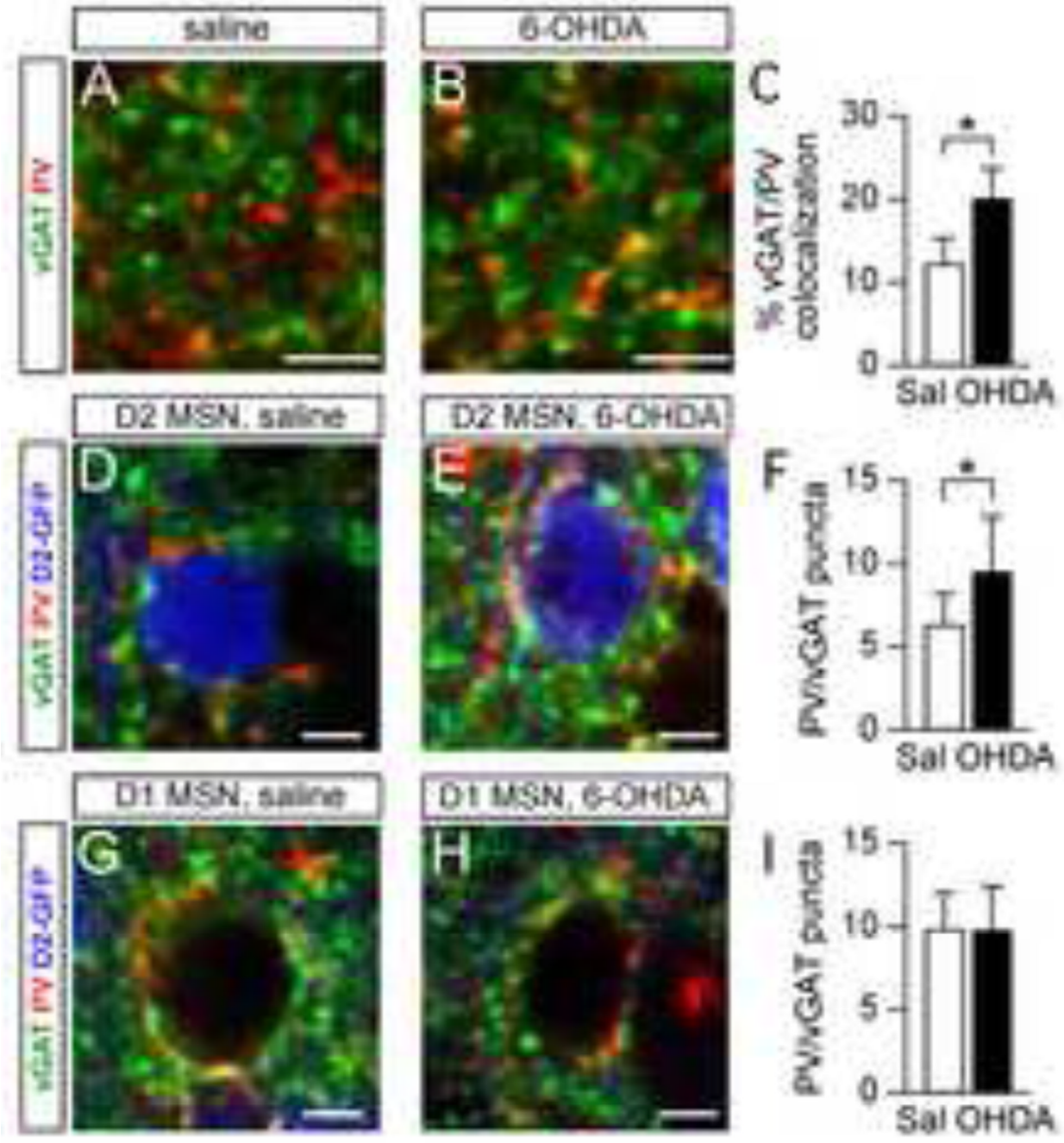

Figure 4. Target-specific increase in inhibitory terminals from FS interneuron after dopamine depletion

A–B. Confocal images showing immunostains against the inhibitory presynaptic marker vGAT, and the FS interneuron marker, PV in sections from saline (A) and 6-OHDA-injected mice (B). All images were pseudocolored to better visualize vGAT/PV colocalization. Scale bars are 5 μm. **C.** Bar graph showing the percentage of vGAT-labeled pixels that were also labeled by PV. The colocalization of these two markers was significantly increased in 6-OHDA-injected mice relative to saline-injected mice, suggesting an increase in inhibitory terminals from FS interneurons. *$p < 0.0001$. **D–E.** Confocal image of basket-like synapses around the soma of D2 MSNs in sections from saline- (D) or 6-OHDA-injected mice (E).

Scale bars are 5 μm. **F.** Bar graph showing an increase in the number of vGAT terminals that were co-labeled with PV around the somas of D2 MSN in 6-OHDA-injected mice compared to saline-injected mice. *p = 0.003. **G–H.** Confocal image of basket-like synapses around the soma of D1 MSNs in sections from saline- (G) or 6-OHDA-injected mice (H). Scale bars are 5 μm. **I.** Bar graph showing no change in the number of vGAT terminals that were co-labeled with PV around the somas of D1 MSNs in 6-OHDA injected mice compared to saline-injected mice.

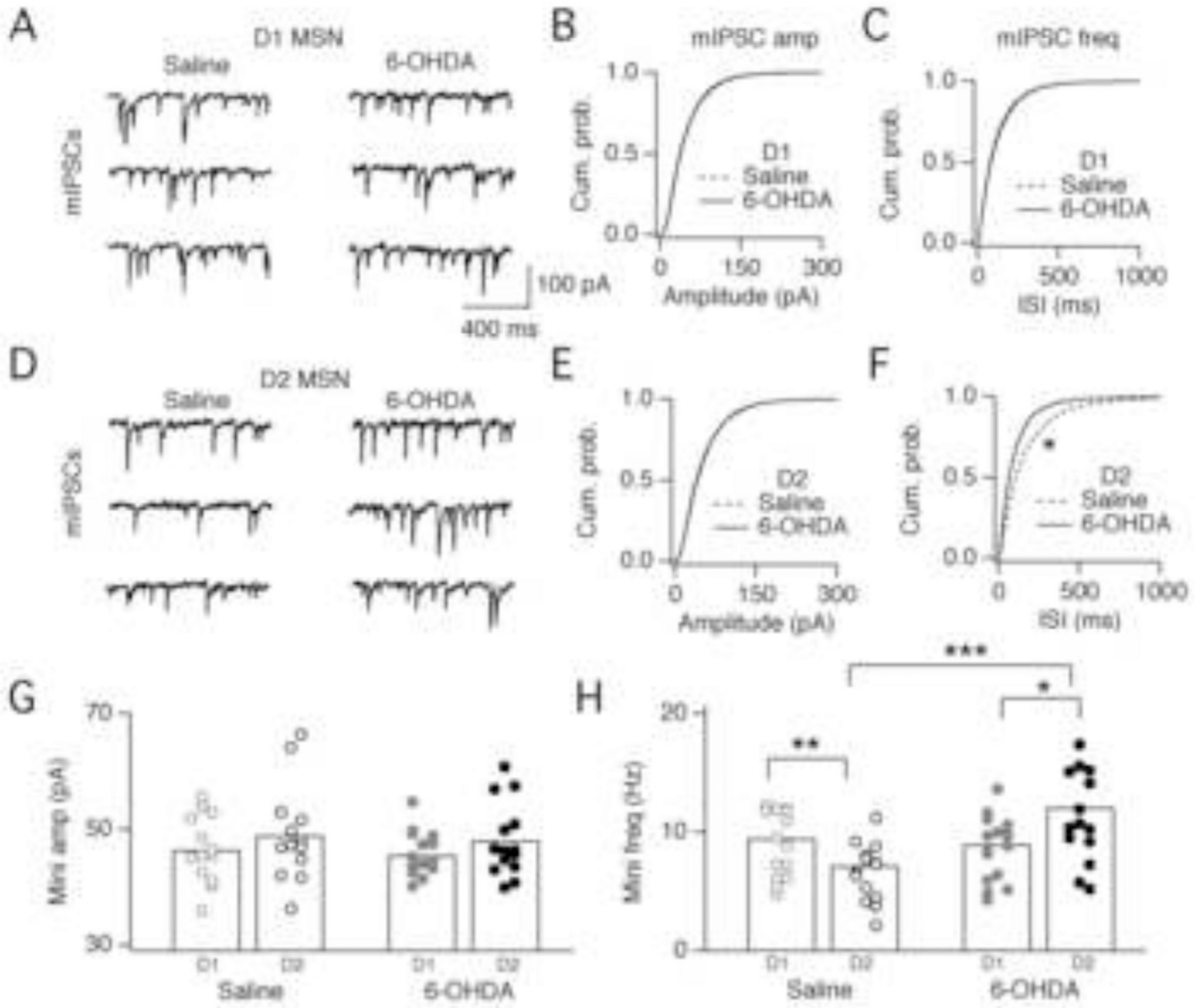

Figure 5. Inhibitory mini frequencies measured in D1 and D2 MSNs

A. Example traces of mIPSCs recorded from D1 MSNs in saline-injected (*left*) or 6-OHDA-injected (*right*) mice. mIPSCs were recorded in the presence of 5 μM NBQX and 1 μM TTX. MSNs were voltage clamped at −80 mV. Due to high [Cl^-] in the internal, E_{Cl} = 0 mV and mIPSCs are inward. **B**. Cumulative probability plot of mIPSC amplitude onto D1 MSNs in saline-injected and 6-OHDA-injected mice. **C.** Cumulative probability plot of mIPSC inter-event interval (isi) recorded in D1 MSNs in saline-injected and 6-OHDA-injected mice. **D.** Example traces of mIPSCs recorded from D2 MSNs in saline-injected (*left*) or 6-OHDA-injected (*right*) mice. **E**. Cumulative probability plot of mIPSC amplitude onto D2 MSNs in saline-injected and 6-OHDA-injected mice. **F.** Cumulative probability plot of mIPSC isi recorded in D1 MSNs in saline-injected and 6-OHDA-injected mice. The mIPSC isi was significantly shorter in D2 MSNs recorded in 6-OHDA-injected mice relative to saline-injected mice (*$p < 0.0001$, Kolmogorov-Smirnov test). **G.** Bar graph summarizing mIPSC amplitudes for the population of D1 and D2 MSNs recorded in saline-injected and 6-OHDA-injected mice. Circles represent data from individual cells and bars are the average

for each population. Amplitudes were not significantly different across conditions. $D1_{saline}$ = 46.5 ± 5.6 pA, n = 14; $D2_{saline}$ = 49.0 ± 8.1 pA, n = 14; $D1_{6\text{-}OHDA}$ 45.7 ± 3.9 pA, n = 15; $D2_{6\text{-}OHDA}$ = 48.1 ± 6.4 pA, n = 14. **H**. Bar graph summarizing mIPSC frequencies for the population of D1 and D2 MSNs recorded in saline-injected and 6-OHDA-injected mice. mIPSC frequencies were significantly higher onto D2 MSNs in 6-OHDA-injected mice compared to saline-injected mice (*p = 0.04; **p = 0.02; ***p = 0.007). $D1_{saline}$ = 9.0 ± 2.8 Hz, n = 14; $D2_{saline}$ = 6.6 ± 2.5 Hz, n = 14; $D1_{6\text{-}OHDA}$ 8.6 ± 2.7 Hz, n = 15; $D2_{6\text{-}OHDA}$ = 11.3 ± 3.8 Hz, n = 14.

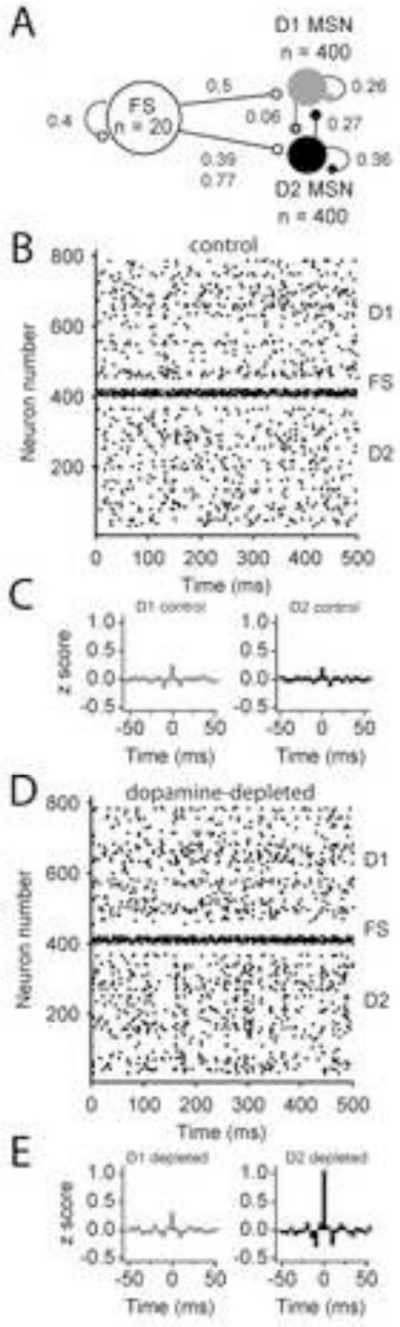

Figure 6. Increased innervation of D2 MSNs by fast-spiking interneurons promotes synchrony in a model of the striatal circuit

A. Diagram of synaptic connections in the model and the connection probability of each. Loops indicate lateral connections onto the same MSN subtype, not autapses. The conductance of all FS synapses was set to 1 nS and the conductance of all MSN synapses was set to 0.2 nS. **B.** Raster plot showing the firing of each neuron in the control network in response to input, simulated by a Gaussian noise function with a standard deviation of 100 pA. **C.** Normalized average cross-correlogram for the population of D1 MSNs and D2 MSNs. The normalized cross-correlogram was computed from data rebinned into 5 ms and converted to a z-score. **D.** Raster plot showing the firing of each neuron in the dopamine-

depleted network in response to input, simulated by a Gaussian noise function with a standard deviation of 100 pA. **E.** Normalized average cross-correlogram for the population of D1 and D2 MSNs. Data was binned into 5 ms bins and converted to a z-score. Note the marked increased in synchrony apparent in the population of D2 MSNs.